UCRL-JC-130818
PREPRINT

An Active and Passive Computed Tomography Algorithm with a Constrained Conjugate Gradient Solution

Jessie A. Jackson
Dennis Goodman
G. Patrick Roberson
Harry E. Martz

This paper was prepared for submittal to the
6th Nondestructive Assay Waste Characterization Conference
Salt Lake City, UT
November 17-19, 1998

October 1998

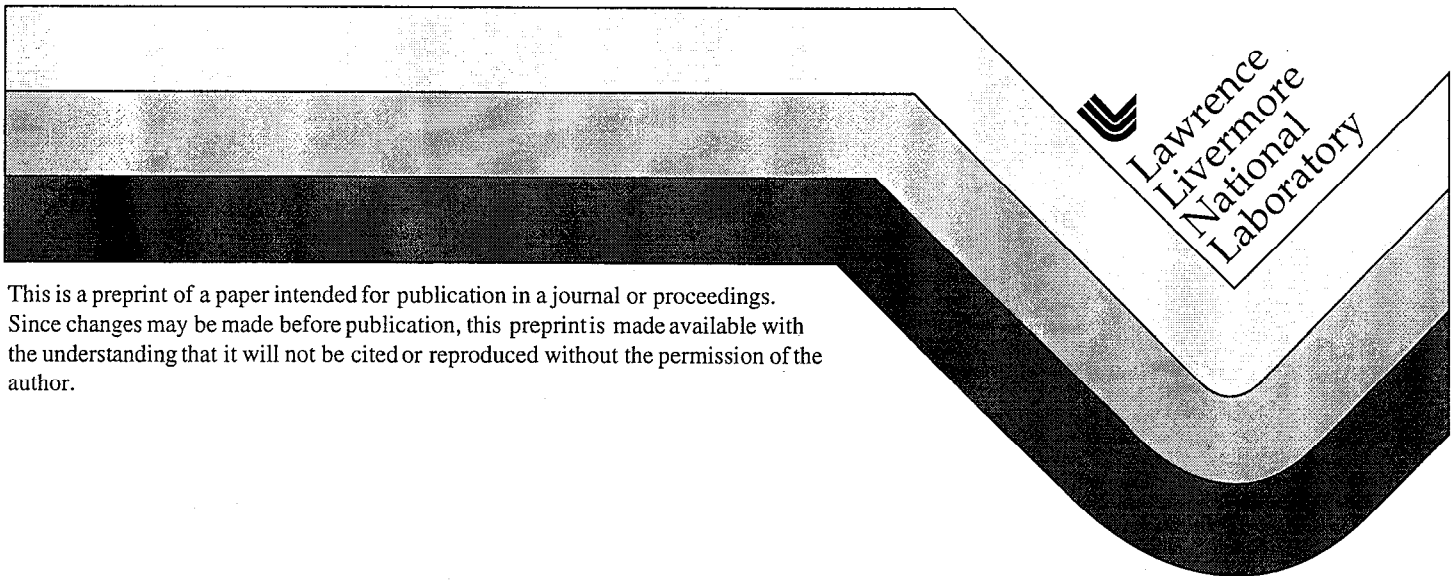

AN ACTIVE AND PASSIVE COMPUTED TOMOGRAPHY ALGORITHM WITH A CONSTRAINED CONJUGATE GRADIENT SOLUTION

Jessie A. Jackson, Dennis Goodman,
G. Patrick Roberson, and Harry E. Martz
Lawrence Livermore National Laboratory
P.O. Box 808, Mail Stop L-333
Livermore, CA 94550, USA
jackson7@llnl.gov

ABSTRACT

An active and passive computed tomographic technique (A&PCT) has been developed at the Lawrence Livermore National Laboratory (LLNL). The technique uses an external radioactive source and active tomography to map the attenuation within a waste drum as a function of mono-energetic gamma-ray energy. Passive tomography is used to localize and identify specific radioactive waste within the same container., The passive data is corrected for attenuation using the active data and this yields a quantitative assay of drum activity.

A&PCT involves the development of a detailed system model that combines the data from the active scans with the geometry of the imaging system. Using the system model, iterative optimization techniques are used to reconstruct the image from the passive data. Requirements for high throughput yield measured emission levels in waste barrels that are too low to apply optimization techniques involving the usual Gaussian statistics. In this situation a Poisson distribution, typically used for cases with low counting statistics, is used to create an effective maximum likelihood estimation function. An optimization algorithm, Constrained Conjugate Gradient (CCG), is used to determine a solution for A&PCT quantitative assay. CCG, which was developed at LLNL, has proven to be an efficient and effective optimization method to solve limited-data problems. A detailed explanation of the algorithms used in developing the model and optimization codes is given.

INTRODUCTION

The goal of the active and passive computed tomography (A&PCT) system is to develop a general purpose method to identify and accurately quantify all the detectable radioisotopes in a closed waste drum. This paper will describe the reconstruction algorithms used to develop a 3-dimensional image of the radioisotopes in a specified spectral region of interest inside the waste drum. The assay of the waste drum can be determined from this 3-dimensional image.

A conceptual design of the A&PCT system is shown in Figure 1. The basic components of the system are the imaging system, filtered back-projection (FBP), isotopic analysis, and the passive reconstruction code. In order to understand the passive reconstruction code, it is necessary to examine pertinent components of the rest of the system and the inputs to the passive reconstruction code. The inputs to the passive reconstruction code are an attenuation image of the waste drum from an active scan of the waste drum, the geometry of the passive scan, measurements of gamma-ray emissions in a spectral region of interest defined by the isotopic analysis and user supplied constraints on the values of the reconstructed image.

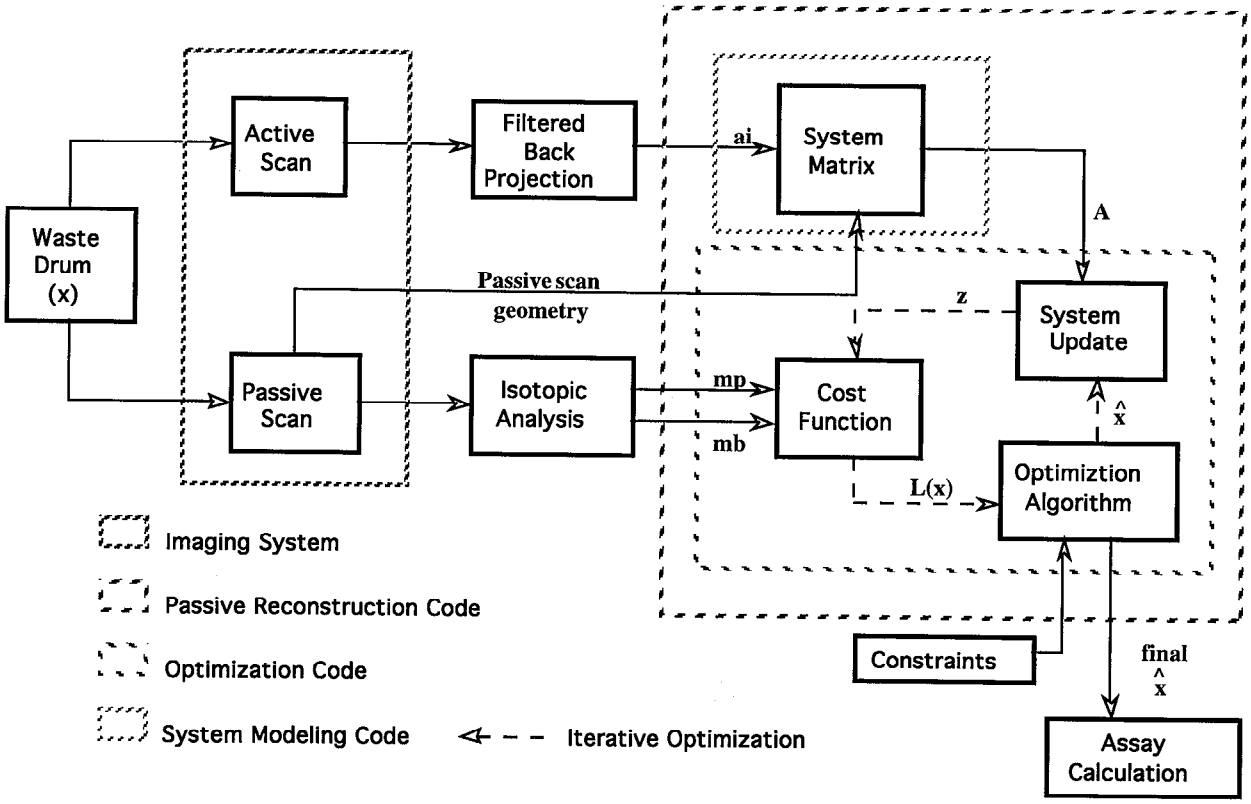

Figure 1: Schematic Design of A&PCT Data Processing

The imaging system consists of a source-detector system and a rotating stage, as shown in Figure 2. A drum to be scanned is placed at the center of the stage. The source-detector system can move across the stage linearly with a total of *ndetectors* locations. The stage can rotate to *nviews* positions and it can also

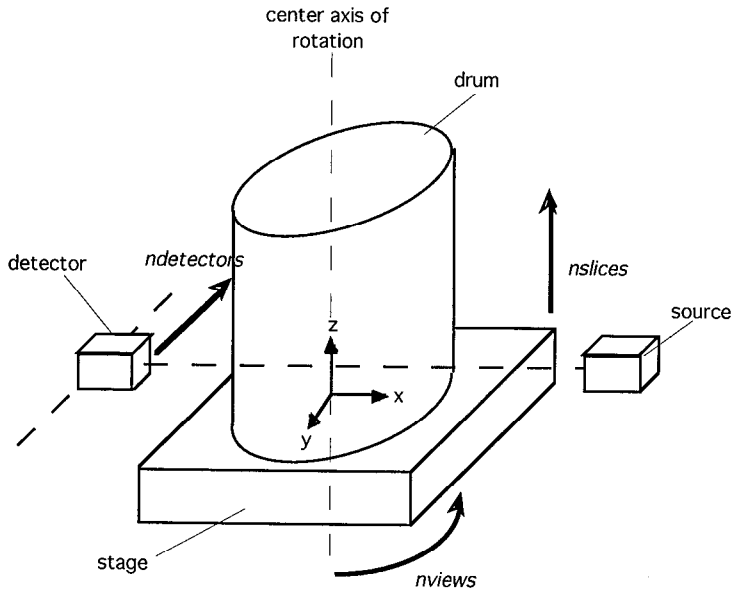

Figure 2: Imaging System

more up and down with *nslices* positions. In order to reduce confusion, from this point on it is assumed that the detector-source system is rotating and elevating and the waste drum and stage are stationary. The appropriate translations are made in the code to make this shift valid.

The attenuation image is determined from an active scan of the drum. The active scan uses an external radioactive source with energies near the peak(s) of interest and a detector. An active scan is performed at each slice position and an image of the linear attenuation coefficient, μ, for that slice is produced by reconstructing the data using a filtered back-projection (FBP)[1] algorithm. The slice images are then combined to produce a 3-dimensional attenuation image. This image data is shown in Figure 1 as the signal **ai**. The image is divided into discrete volumes called voxels. The dimensions of the image in voxels are *nx, ny,* and, *nz,* where *(x, y, z)* correspond to the axis shown in Figure 1. The sizes of the voxels in each direction are *dx, dy,* and *dz.* The origin position of the first voxel is *(xo, yo, zo).* Typical attenuation image values for a waste drum are $nx = ny = 14$, $nz = 17$, $dx = dy = dz = 50.8$mm, and $xo = yo = -330.2$mm, $zo = 0.0$mm. The actual detector-source positions used during the active scan are not needed in the passive reconstruction code, however they do define the size of the attenuation image voxels. The reconstructed emission image have the same dimensions as the attenuation image. Therefore the detector-source movements during the active scan must be selected with the size of the emission image in mind.

During the passive scan only the detector is used to collect the gamma-ray emission, i.e. no external source is required. The scan is produced by the detector moving in the same manner as the active scan, though the actual step size and number of positions can be different. The detector scans each vertical

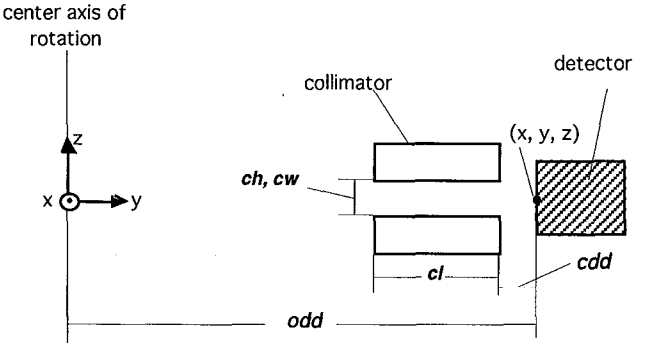

Figure 3: Imaging System Dimensions for Passive Scan

position slice by slice. For each slice, the detector starts at the initial position and moves along the linear path, then rotates to a new position and moves linearly again. The important dimensions of the imaging system that are used for the passive scan are shown in Figure 3. These dimensions include the collimator

length, *cl*, the collimator width and height, *cw* and *ch*, the distance from the detector face to the center axis of the drum rotation, *odd*, and the distance from the detector face to the collimator, *cdd*. Other information that is needed for the reconstruction involves the position of the detector at each scan location relative to the xyz coordinate system. The initial vertical slice location, *slice1*, is given relative to the z-axis. The initial position of angular rotation, or view, *view1*, is given relative to the y-axis. The initial position of the detector, *det1*, is at the beginning of the horizontal linear line of movement. The number of steps for each movement are given as *ndetectors*, *nviews*, and *nslices*. The sizes of each step are Δd, Δv, and Δz. Typical passive scan values for a waste drum are *ndetectors* = 7 or 14, *nviews* = 10 or 21, *nslices* = 17, Δd = 50.8 or 101.6mm, Δv = 36.0 or 17.15, Δz = 0.0mm, *det1* = -330.2mm, *view1* = 0.0, and *slice1* = 0.0.

The passive reconstruction code uses as input data from the passive scan has already been processed by n isotopic analysis. The isotopic analysis has as input the sum of all gamma-ray counts for all the spectral channels. The isotopic analysis extracts peaks from specified spectral regions of interest. The passive reconstruction code produces an reconstructed emission image for only one gamma peak at a time. This is the peak selected by the isotopic analysis. The raw signal is of the form shown in Figure 4. The data is collected in discrete spectral channels. The signal of interest consists of a background component and a net component. The net component is produced by selected radioisotopes of interest. The goal of the passive reconstruction code is to determine the source activity that causes the net component. The isotopic analysis provides the passive reconstruction code with two signals. One signal is the sum of three spectral channels on each side of the peak, where there is no interference from the peak of interest or any other peak of interest. This signal is called the background measurement, shown in Figure 4 as **mb**. The other signal is the sum of the spectral channels under the peak. This signal is called the peak measurement, **mp**. The other information the isotopic analysis provides to the reconstruction code is the number of channels under the peak, *npeak*, and the number of channels used in the background measurement, *nbkgnd*. The background measurement can be determined in other ways as long as the information provided to the passive reconstruction code is equivalent and *nbkgnd* is correct.

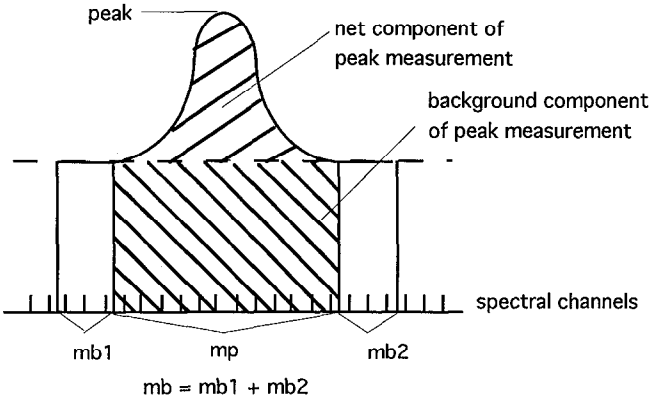

Figure 4: Passive Signal Components

The final input information supplied to the passive reconstruction code are constraints on the range of

values the reconstructed emission image is allow to have. Minimum and maximum values for each image voxel can be selected. In the waste drum case however the only constraint is that the emission image values must be non-negative.

PASSIVE RECONSTRUCTION CODE

The problem to be solved is of the form $\mathbf{z(x) = A \bullet x}$, where **x** is a vector to be solved for and **z(x)** is a vector of measured values. **A** is a system matrix which relates **x** to **z(x)**. In the case where **A** is too large to invert an iterative optimization process can be used to solve for **x**. The iterative technique used in A&PCT is shown in the conceptual design of the passive reconstruction code in Figure 1. The iterative solution process starts with an initial guess $\hat{\mathbf{x}}$ for the value of **x**, then $\hat{\mathbf{z}}(\mathbf{x}) = \mathbf{A} \cdot \hat{\mathbf{x}}$ is calculated. A cost function, **L(x)**, compares the measured **z** to the calculated $\hat{\mathbf{z}}$. If the stopping criteria are not satisfied the optimization algorithm searches for a value of $\hat{\mathbf{x}}$ that reduces **L(x)** further and the process is repeated. In order to use this iterative optimization method three components must be defined: the system matrix **A**, an appropriate cost function **L(x)**, and an effective optimization algorithm. In the waste drum case the system model provides a means to calculate $\mathbf{z(x) = A \bullet x}$, the net counts at each detector produced by the source activity represented by **x**. Unfortunately **z(x)** can not be measured. The measured values from the passive scan are the peak and background counts, **mp**, and **mb**. A cost function has been constructed to relate **z(x)** to **mp** and **mb**.

The passive reconstruction code, as seen in Figure 1, is divided into two code sections, the system model code and the optimization code. The system model code calculates the system matrix **A**. The optimization code includes the cost function calculation and the optimization algorithm. The optimization algorithm used in A&PCT is called Constrained Conjugate Gradient (CCG).

SYSTEM MATRIX

The waste drum system is represented by $\mathbf{z(x) = A \bullet x}$, where **x** is the vector representing the reconstructed emission image voxels, and **z** is the vector representing the emission counts that reach the detector positions. Each element, A_{dv}, of the matrix **A** represents the portion of the counts from emission image voxel v that reaches detector position d.

The collimator in front of the detector is to creates a relatively narrow field-of-view through the waste drum as seen from each detector. In other words many values of A_{dv} are zero for a given d because of the collimator restricted view of the detector. One approach to determining the **A** matrix is to examine each

element of **A**, decide whether the voxel position is seen by the detector and if it is determine the effect of the attenuation. The attenuation can be determined by finding the path from the voxel to the detector and then calculating the line integral of the attenuation along that path. This method is rather complicated and inefficient so a different approach will be used.

The approach in A&PCT is to start with a detector and divide the area it sees, into discrete rays, both vertically and horizontally. Figure 5 shows a view of this process for a single z slice of a drum. The processing moves out along the center of each ray with a given step size. At each step point the attenuation to that point is calculated. In this case calculating the attenuation is relatively simple since the total attenuation line integral is the attenuation to the previous step point plus the additional attenuation from the previous to the current step point. Other values, such as ray volume, and point-spread function are also be calculated at each step point. The image voxel, *v*, that the step point is in is determined and the corresponding value of A_{dv} is updated. A given A_{dv} can be the sum of components from a number of step points along one ray, as well as contributions from adjacent rays.

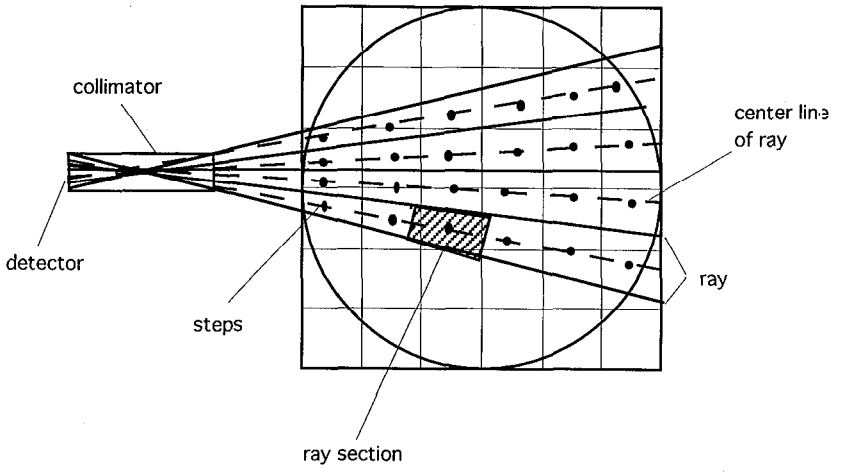

Figure 5: Detector Field-of-View Segmented into Rays with Processing Steps and Ray Sections

The following describes the details involved in determining the ray sections, the step size, the movement along the ray, and the calculations involved in determining the contribution at each step position to the system matrix **A**.

In order to make sure the image and the measurements are aligned to the xyz coordinate system the center of rotation, (*ctrx, ctry*) is calculated as in Equations 1a and 1b.

$$ctrx = dx \cdot \frac{(nx-1)}{2} + xo \qquad (1a)$$

$$ctry = dy \cdot \frac{(ny-1)}{2} + yo \qquad (1b)$$

A value called *rr*, defines the radius of a circle, within which a complete image exists. *rr* is calculated by finding the radius that will allow the largest complete circle within image grid.

$$rr = \min\left(dx \cdot \frac{nx}{2}, dy \cdot \frac{ny}{2}\right) \qquad (2)$$

The number of rays along which the attenuation line integral is calculated is defined by a value called *nsub*. The number of rays will be the same horizontally and vertically. *nsub* is selected so that there are 2 rays per image voxel at the farthest end of the ray, the far side of the image. The physical setup for determining *nsub* is shown in Figure 6. The calculation for *nsub* is in Equation 3.

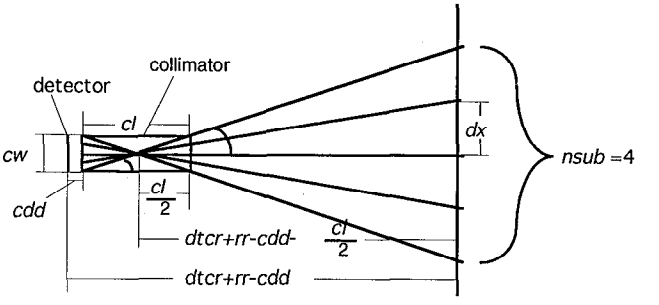

Figure 6: Physical Values Used for the Calculation of *nsub*

$$nsub = 2 \cdot \text{int}\left[\left(\frac{2(dtcr + rr - cdd)}{cl} - 1\right) \cdot \frac{cw}{dx} + 0.5\right] \tag{3}$$

Individual ray angular width and height, $\Delta\phi_w$ and $\Delta\phi_h$, are calculated by dividing the total angular width and height of detector field-of-view by the number of rays. The total angular width and height of the field-of-view of the detector are dependent on the collimator dimensions.

$$\Delta\phi_w = \frac{2}{nsub} \cdot \tan^{-1}\left(\frac{cw}{cl}\right) \tag{4a}$$

$$\Delta\phi_h = \frac{2}{nsub} \cdot \tan^{-1}\left(\frac{ch}{cl}\right) \tag{4b}$$

The center line of each ray is the line the line integral will be calculated along. The ray center is specified by the angular position relative to the collimator axis, the line through the center of the collimator. Two angles are used to define the ray position. One angle, δ_l, fan-angle-left, specifies the position in the x-y plane and the other angle, δ_u, fan-angle-up, specifies the position in the z-collimator axis plane. The equations for the fan-angles are given in Equations 5a and 5b, where *ir* and *jr* = 0, 1, ... (*nsub*-1). A diagram of the values used in determining δ_l is shown in Figure 7.

$$\delta_u = \frac{\phi_h}{2} - \frac{\Delta\phi_h}{2} - jr \cdot \Delta\phi_h \tag{5a}$$

$$\delta_l = \frac{\phi_w}{2} - \frac{\Delta\phi_w}{2} - ir \cdot \Delta\phi_w \tag{5b}$$

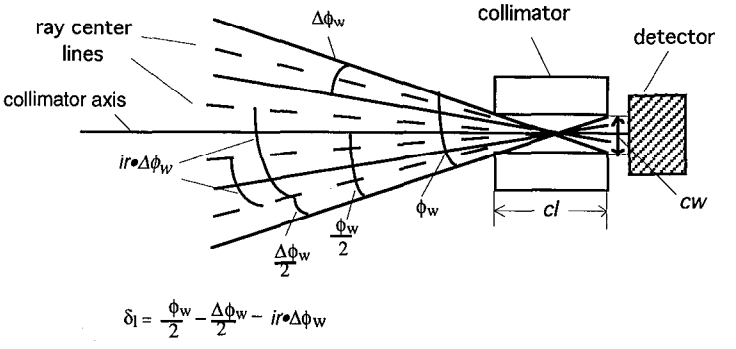

Figure 7: Ray Center Line Determination

If the origin of the coordinates is in the middle of a pixel, then the bottom of the barrel is *dz*/2 below the origin and the top is *dz*/2 above the last pixel, so the limits *ztop* and *zbottom* are needed.

$$zbottom = zo - dz/2 \tag{6a}$$

$$ztop = zo + (nz - 1) \cdot dz + dz/2 \tag{6b}$$

In order to relate the attenuation image to the passive measurements the detector positions are needed on the xyz coordinate system. The first step in this process is to determined the relative detector position, given the sampling information shown in Figure 8.
Note that θ = *view_angle.*

$$r = id \cdot \Delta d + d1 \tag{7a}$$

$$view\_angle = iv \cdot \Delta view + view1 \tag{7b}$$

$$zslice = iz \cdot \Delta slice + slice1 \tag{7c}$$

where
id = 0, 1, ... *ndetectors*
iv = 0, 1, ... *nviews*
iz = 0, 1, ... *nslices*

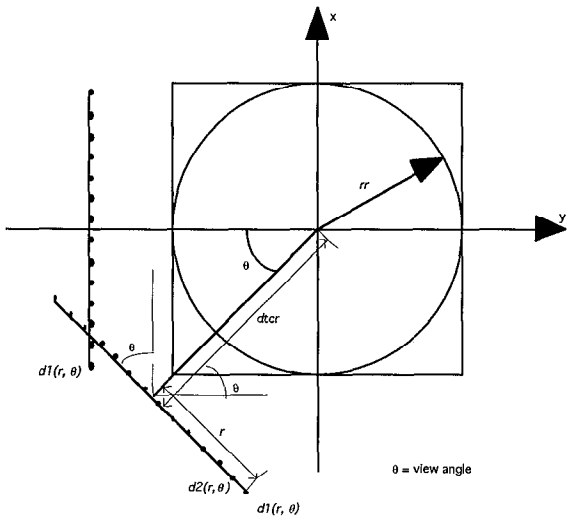

Figure 8: Detector Movements

The detector position is translated to the (x,y,z) coordinate system. Figure 9 shows the relationship between the relative detector positions and the xyz coordinate system. The equations for translation are given in Equations 8a through 8b. The *(ctrx, ctry)* values align the detector positions with the attenuation image.

$$x = r \cdot \cos\theta - dtcr \cdot \sin\theta + ctrx \tag{8a}$$

$$y = -r \cdot \sin\theta - dtcr \cdot \cos\theta + ctry \tag{8b}$$

$$z = z \tag{8c}$$

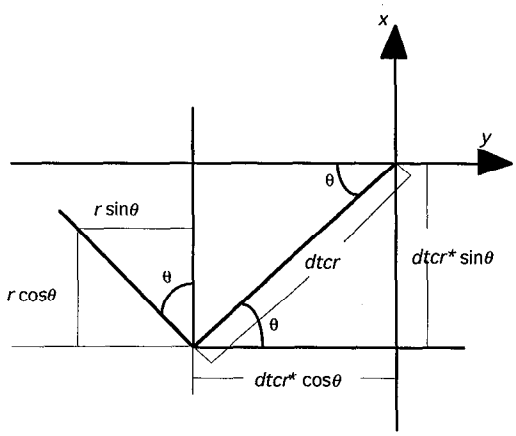

Figure 9: Detector Position Coordinate Translation

Once the detector position is determined, the attenuation line integral along each ray is calculated. The program increments from ray to ray and for each ray it steps the length of the ray. Figure 10 shows the

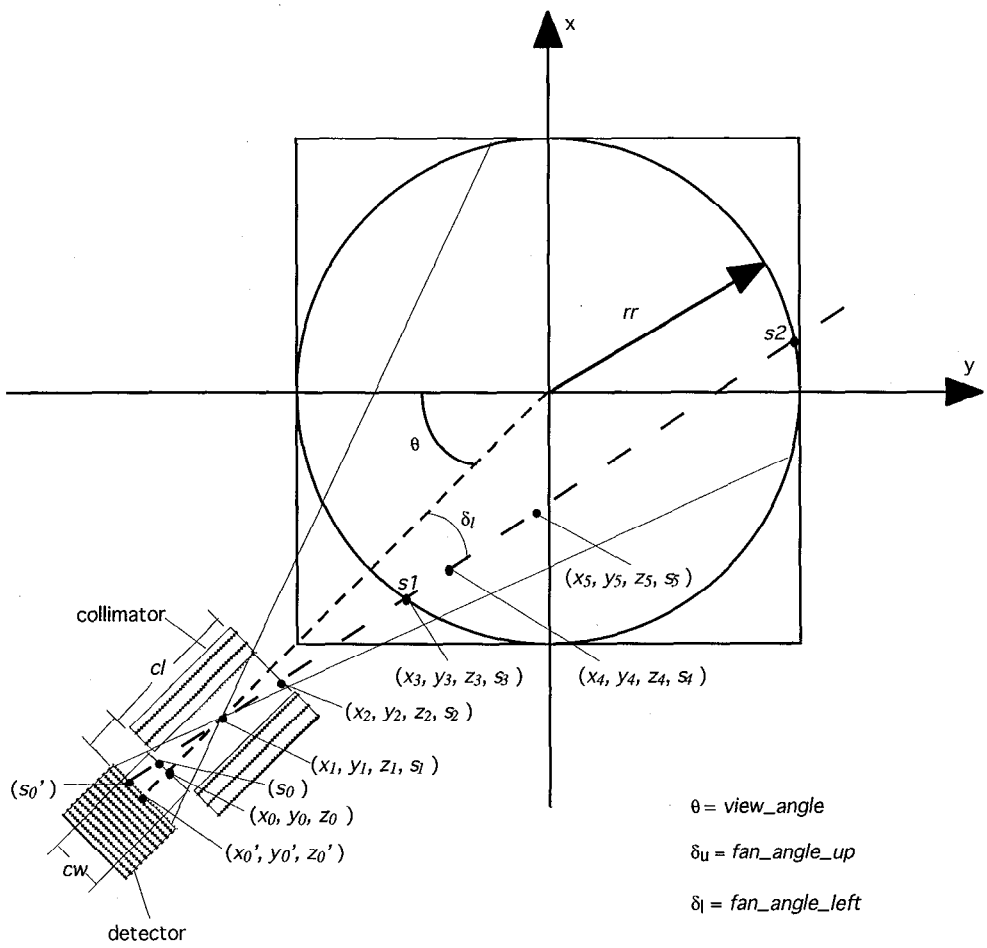

Figure 10: Processing Steps on the Ray Center Line

steps involved in this process. Two sets of location values must be calculated; the (x,y,z) position coordinate and *s*, the distance from the detector. The initial coordinate position, (x_0', y_0', z_0'), is calculated as shown in Equations 8a-c. The position is the center of the detector on the collimator axis. The initial position of *s*, $s_0' = 0$, is on the detector face at the location of the intersection of the ray center line with the detector face.

The first step moves to the end of collimator. *s* moves along the ray to s_0 and (x, y, z) moves along the collimator axis to (x_0, y_0, z_0). The equations for this movement are given in Equations 9a - d.

$$x_0 = x_0' + cdd \cdot \sin\theta \tag{9a}$$

$$y_0 = y_0' + cdd \cdot \cos\theta \tag{9b}$$

$$z_0 = z_0' \tag{9c}$$

$$s_0 = s_0' + cdd \cdot \frac{1}{\cos\delta_u \cdot \sin\delta_l} \tag{9d}$$

The next step is to the center of the collimator. Again, s, moves along the ray to s_1, and (x,y,z) moves along the collimator axis to (x_1, y_1, z_1).

$$x_1 = x_0 + \frac{cl}{2} \cdot \sin\theta \tag{10a}$$

$$y_1 = y_0 + \frac{cl}{2} \cdot \cos\theta \tag{10b}$$

$$z_1 = z_0 \tag{10c}$$

$$s_1 = s_0 + \frac{cl}{2} \cdot \frac{1}{\cos\delta_l \cdot \cos\delta_u} \tag{10d}$$

The next step is to the front end of the collimator. From this point on both s and (x, y, z) will follow the ray. Equations 11a-d describe the movement to (x_2, y_2, y_2, s_2), the front end of the collimator.

$$x_2 = x_1 + \sin(\theta + \delta_l) \cdot \frac{cl}{2} \cdot \frac{1}{\cos\delta_l} \tag{11a}$$

$$y_2 = y_1 + \cos(\theta + \delta_l) \cdot \frac{cl}{2} \cdot \frac{1}{\cos\delta_l} \tag{11b}$$

$$z_2 = z_1 + \frac{cl}{2} \cdot \frac{\sin\delta_u}{\cos\delta_u \cdot \cos\delta_l} \tag{11c}$$

$$s_2 = s_1 + \frac{cl}{2} \cdot \frac{1}{\cos\delta_l \cdot \cos\delta_u} \tag{11d}$$

The steps from now on involve determining a distance of movement in s. This movement is translated to (x, y, z). The easiest way to do this is to determine a change in x, y and z for a unit change in s. These values are given by *dxds, dydx,* and *dzds*. The values for these variables are given in Equations 12a-c.

$$dxds = \sin(\theta + \delta_l) \cdot \cos\delta_u \tag{12a}$$

$$dyds = \cos(\theta + \delta_l) \cdot \cos\delta_u \tag{12b}$$

$$dzds = \sin\delta_u \tag{12c}$$

The next movement steps along the ray to the beginning of the recon-circle, the circle defined by the recon-radius variable *rr*. In order to make this step the point where the ray center line intersects the recon circle in the (x, y) plane is determined. The intersection needs to be calculated in terms of s only. The intersection points are *s1* and *s2*. *s1* and *s2* are the distances from the current location (x_2, y_2, z_2). Figure 11 shows the geometry involved.

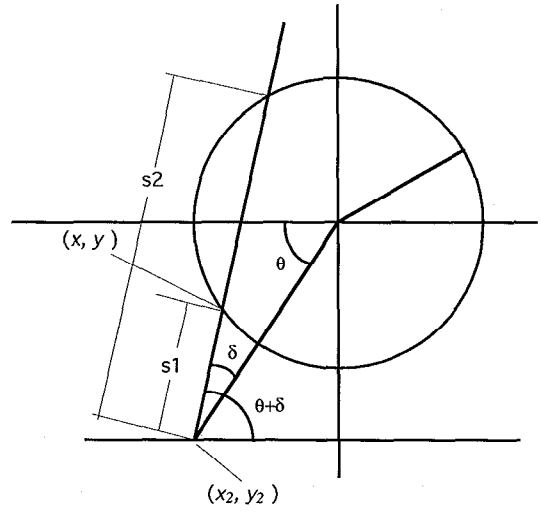

Figure 11: Ray and Recon Circle Intersection

The line is described by Equations 13a-b, and the circle is described by Equation 13c.

$$(x - x_2) = s \cdot \sin(\theta + \delta_l) \cdot \cos\delta_u \quad (13a)$$

$$(y - y_2) = s \cdot \cos(\theta + \delta_l) \cdot \cos\delta_u \quad (13b)$$

$$x^2 + y^2 = rr^2 \quad (13c)$$

The solution is found by solving the quadratic equation. The quadratic variables *a, b, c* are given in Equations 14a-c and the solutions *s1* and *s2* are given in Equations 15a-b.

$$a = dxds^2 + dyds^2 \quad (14a)$$

$$b = 2 \cdot (x_2 \cdot dxds + y_2 \cdot dyds) \quad (14b)$$

$$c = x_2^2 + y_2^2 - rr^2 \quad (14c)$$

$$s1 = \frac{-b - \sqrt{b^2 - 4ac}}{2a} \quad (15a)$$

$$s2 = \frac{-b + \sqrt{b^2 - 4ac}}{2a} \quad (15b)$$

If $(b^2\text{-}4ac) < 0$ the ray is outside the recon circle and no further processing is needed on this ray. If $s1 > s2$ switch *s1* and *s2*.

The other condition that needs to be checked is the position of *s1* and *s2* relative to the outside bounds of *z*, *zbottom* and *ztop*. First calculate the *z* values for *s1* and *s2*. If *zs2* > *ztop* or *zs1* < *zbottom*, recalculate *s1* or *s2* to reflect the actual top or bottom of the drum.

$$zs1 = z + dzds \cdot s1 \quad (16a)$$

$$zs2 = z + dzds \cdot s2 \quad (16b)$$

$$\text{if}(zs1 < zbottom) \quad s1 = (zbottom - z_2)/dzds \quad (17a)$$

$$\text{if}(zs2 < zbottom) \quad s2 = (zbottom - z_2)/dzds \quad (17b)$$

$$\text{if}(zs1 > ztop) \quad s1 = (ztop - z_2)/dzds \quad (17c)$$

$$\text{if}(zs2 > ztop) \quad s2 = (ztop - z_2)/dzds \quad (17d)$$

Now the step is made to *s1*. The coordinates are (x_3, y_3, z_3, s_3) and they are calculated in Equations 18a-d.

$$x_3 = x_2 + s1 \cdot dxds \quad (18a)$$

$$y_3 = y_2 + s1 \cdot dyds \quad (18b)$$

$$z_3 = z_2 + s1 \cdot dzds \quad (18c)$$

$$s_3 = s_2 + s1 \quad (18d)$$

Before beginning to step along the ray in the recon circle a step size needs to be determined. The step size equals the width of a ray at the center of rotation. The total width of the detector field-of-view is *ctrw*. The geometry is shown in Figure 12. The calculation for the step size, Δs, is given in Equation 19.

$$\Delta s = \frac{2}{nrw} \cdot \frac{cw}{cl} \cdot \left(dtcr - \frac{cl}{2} - cdd \right) \qquad (19)$$

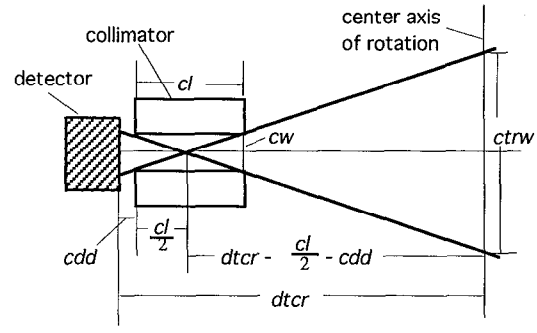

Figure 12: Step Size Calculation

The first step size is $\Delta s/2$ so that (x, y, z) will always be in the middle to the Δs step. So the location for the first place the a value for the system matrix is calculated is (x_4, y_4, z_4, s_4), as shown in Equations 20a-d.

$$x_4 = x_3 + \Delta s/2 \cdot dxds \qquad (20a)$$
$$y_4 = y_3 + \Delta s/2 \cdot dyds \qquad (20b)$$
$$z_4 = z_3 + \Delta s/2 \cdot dzds \qquad (20c)$$
$$s_4 = s_3 + \Delta s/2 \qquad (20d)$$

The following step is in Δs increments, as shown in Equations 21a-d. Progress along the ray stops when $s > s2$.

$$x_5 = x_4 + \Delta s \cdot dxds \qquad (21a)$$
$$y_5 = y_4 + \Delta s \cdot dyds \qquad (21b)$$
$$z_5 = z_4 + \Delta s \cdot dzds \qquad (21c)$$
$$s_5 = s_4 + \Delta s \qquad (21d)$$

The location (x, y, z, s) needs to be mapped onto the image grid, (ii, jj, kk). Figure 13 shows the relationship between (x, y, z) and the image bins, (ii, jj), on the x-y plane. (xo, yo, zo) is the location of the image origin. Equations 22a-c show the equations for the translation

$$ii = \frac{(x - xo + dx/2)}{dx} \qquad (22a)$$

$$jj = \frac{(y - yo + dy/2)}{dy} \qquad (22b)$$

$$kk = \frac{(z - zo + dz/2)}{dz} \qquad (22c)$$

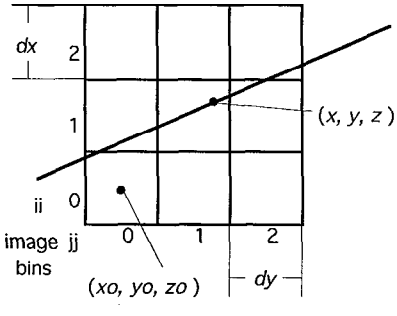

Figure 13: Translation to Image Grid

At each step on the ray the volume of the segment at that point is calculated. The cross section of a ray section is shown in Figure 14. The length of the segment is Δs. The area of the segment is determined by finding the area of the detector field of view at distance s, and dividing by the total number of

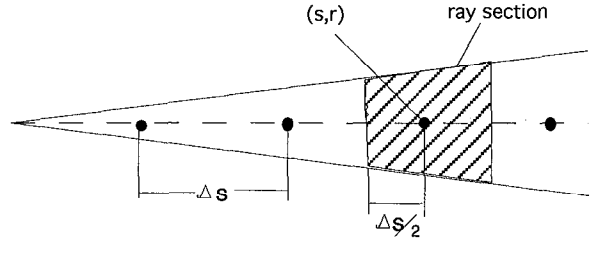

Figure 14: Ray Segment

rays. First s is projected on to the collimator, or optical, axis, as shown in Figure 15. This value is soa, Equation 23a. Then the spread-width, sw, and spread-height, sh, are calculated, Equation 23b-c. Finally the area and then the volume are determined, Equation. 24a-b.

$$soa = s \cdot \cos\delta_u \cdot \cos\delta_l \tag{23a}$$

$$sw = 2 \cdot \frac{cw}{2} \cdot \left(soa - \frac{cl}{2} - cdd \right) \tag{23b}$$

$$sh = 2 \cdot \frac{ch}{2} \cdot \left(soa - \frac{cl}{2} - cdd \right) \tag{23c}$$

$$A_{sr} = \frac{sw \cdot sh}{nrw \cdot nrh} \tag{24a}$$

$$V_{sr} = A_{sr} \cdot \Delta s \tag{24b}$$

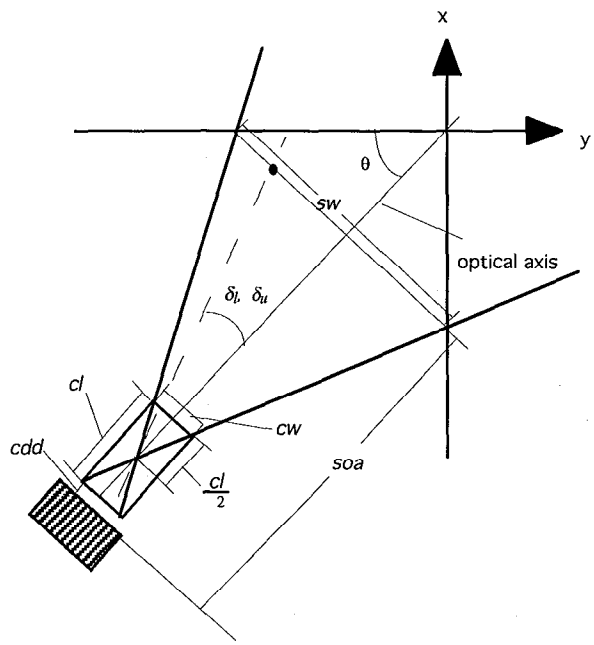

Figure 15: Ray Area

The contribution to **A** at each step applies for the area of the ray around the point. This value to be calculated at each ray-step is D_{sr}, s, refers to the step position along the ray and r refers to the ray. There are two components to D_{sr}:

$$D_{sr} = P_{sr} \cdot B_{sr} \tag{25}$$

The P_{sr} term involves the "probability" that an emission at the location (s,r) will reach the specific detector. The B_{sr} term takes into account the absorption between the detector and the location (s,r). P_{sr} is calculated as:

$$P_{sr} = \frac{SA_s \cdot psf_{sr} \cdot V_{sr}}{SC} \tag{26}$$

The solid angle term, SA_{sr}, represents the ratio of the area of a detector over the total possible area that the emission could reach at a distance s.

$$SA_{sr} = \frac{detector\_area}{4\pi s2} \tag{27a}$$

$$detector\_area = cw \cdot ch \tag{27b}$$

$4\pi s^2$ is the area of the sphere at a distance, s, from the point (s,r).

psf_{sr} is the point-spread function and it is used to take into account the fact that an emitter directly in line with the collimator/detector will impact the detector, but some of those of to the side will enter the collimator but not reach the detector. The V_{sr} term represents the volume of the ray segment where (s,r) is the center point of the ray segment, see Figure 13. SC is a scaling term to convert from mm^3 to bins,

where dx, dy and dz are the dimensions of the image voxels.

$$SC = dx \cdot dy \cdot dz \tag{28}$$

For the absorption term, B_{sr} the line integral exp(-μl) from the edge of the waste drum to the current location, *(s,r)* needs to be determine. A running line integral sum is calculated as the code steps out along each ray. The absorption value, *ai(v),* is the attenuation coefficient from the attenuation image for voxel *v*. vsr_{sr} is the voxel in which the location *(s,r)* is. The absorption term is then

$$B_{sr} = \exp\left\{-\Delta s \sum_{s'}^{S-1} ai\left(vsr_{s'r}\right) - \frac{\Delta s}{2} \cdot ai\left(vsr_{sr}\right)\right\} \tag{29}$$

The term $\Delta s \sum_{s'}^{S-1} ai\left(vsr_{s'r}\right)$ represents the absorption up to the current ray section and $\Delta s/2 \cdot ai\left(vsr_{sr}\right)$ takes care of the first half of the current ray section.

Finally, the actual value of A_{sr} is:

$$A_{sr} = \sum_s \sum_r D_{sr} \tag{30}$$

or

$$A_{sr} = \sum_s \sum_r \left\{ \frac{SA_s \cdot psf_{sr} \cdot V_{sr}}{SC} \cdot \exp\left\{-\Delta s \left[\sum_{s'}^{S-1} ai\left(vsr_{s'r}\right) + \frac{1}{2} ai\left(vsr_{sr}\right)\right]\right\}\right\} \tag{31}$$

COST FUNCTION

A cost function compares an actual measured value with a calculated value. In order to use an optimization search, a cost function must be determined. The success of the optimization procedure depends in large part on the specification of the cost function.

A standard cost function is the least-squares, which assumes a process with Gaussian statistics. Counting data, such as radioactive decay, is statistically represented by a Poisson distribution. A Poisson distribution approaches a Gaussian distribution in the case of large counting values. Since the count level of the data from a waste drum are typically be too low to approach Gaussian statistics, a cost function using the Poisson distribution has been developed.

The probability of n counts in a Poisson probability distribution is given by

$$\Pr\{n\} = \frac{1}{n!} a^n \exp(-a) \tag{32}$$

where the parameter a is the mean or expected value of the counts for the process. The parameters a and

n must be non-negative integers. The value of a characterizes or defines a particular Poisson process, and n is the observed or measured counts from the process. Equation 32 states that the probability, for a given a, that n counts will be observed is $\Pr\{n\}$. In a situation, such as a waste drum, the observation n is known but to characterize the process the mean a must be determined. One way to find a value of a is to search for the value of a that maximizes the probability, $\Pr\{n\}$, that n will be observed. In other words, what value of a will most likely cause the value of n to occur[2].

In the case where there are multiple observations, n will be a vector, **n**, with N elements, where N is the number of observations. Each observation in the vector **n** will have a Poisson distribution and an expected value associated with it. These expected values will form a vector **a** with N elements. To characterize the system, values for all the elements in **a** must be found. The value of **a** should be selected to maximize all the probability distributions. Since the observations are all statistically independent the function to be maximized can be the product of the individual probabilities distributions of all the observations, as in Equation 33.

$$\Pr\{n_1\} \bullet \Pr\{n_2\} \bullet .... \bullet \Pr\{n_N\} \tag{33}$$

This is called a joint probability function. This is the approach that will be applied to the waste drum. To determine the actual cost function values for the waste drum corresponding to the vectors **n** and **a** are defined[3].

In the waste drum the measured values are the peak and background signals mp_k and mb_k for all detector positions k. The system matrix **A** defines the relationship $\mathbf{z(x)} = \mathbf{A} \bullet \mathbf{x}$, where **x** is a vector containing the values of emissions from each image voxel and **z** represents the net counts at each detector. **z(x)** can not be measured. Therefore a relationship between $z_k(\mathbf{x})$ and mp_k and mb_k must be determined. This can be done by first defining variables w_k to be the mean total background counts at each detector k. w_k will be the background counts for all the spectral channels $ntotal = nbkgnd + npeak$. The amount of w_k that is in the background measurement, mb_k, is τ_1 where

$$\tau_1 = \frac{nbkgnd}{ntotal} \tag{34}$$

and the amount in the peak measurement, mp_k is τ_2, where

$$\tau_2 = 1 - \tau_1 = \frac{npeak}{ntotal} \tag{35}$$

Likewise the mean net counts $z_k(x)$, can be divided between mp and mb_k. τ_3 will be the amount of $z_k(x)$ in the background measurement. For the waste drum τ_3 will be zero. τ_4 is the amount of $z_k(x)$ in the peak measurement, which in this case will be one, since

$$\tau_4 = 1 - \tau_3 \tag{36}$$

Where $E\{n\}$ represents the expected value or mean of the process which produces n, the relationships

between mp_k, mb_k, w_k, and $z_k(\mathbf{x})$ are

$$\mathrm{E}\{mb_k\} = \tau_1 w_k + \tau_3 z_k(\mathbf{x}) \tag{37a}$$

$$\mathrm{E}\{mp_k\} = \tau_2 w_k + \tau_4 z_k(\mathbf{x}) \tag{37b}$$

The cost, or likelihood, function for the waste drum can now be formulated. The cost function is based on the joint probability distribution of all the measurements. mp_k and mb_k are the measured values and $\mathrm{E}\{mp_k\}$ and $\mathrm{E}\{mb_k\}$ are the expected values. The joint probability distribution is

$$\Pr(\mathbf{mp},\mathbf{mb},\mathbf{w},\mathbf{x}) = \prod_{k=1}^{K}\left\{\frac{1}{mb_k!}\left[\tau_1 w_k + \tau_3 z_k(\mathbf{x})\right]^{mb_k}\exp\left(\tau_1 w_k + \tau_3 z_k(\mathbf{x})\right)\right\}\bullet \prod_{k=1}^{K}\left\{\frac{1}{mp_k!}\left[\tau_2 w_k + \tau_4 z_k(\mathbf{x})\right]^{mp_k}\exp\left(\tau_2 w_k + \tau_4 z_k(\mathbf{x})\right)\right\} \tag{38}$$

Since it is easier to maximize the log of the Pr(**mp,mb,w,x**) will actually be used. All the terms that are not dependent on **w** and **x** will be removed, leaving the cost function

$$\mathrm{L}[\hat{\mathbf{w}},\hat{\mathbf{x}}] = \left\{\sum_{k=1}^{K}\left(-w_k - z_k(\mathbf{x}) + mp_k\log\left[\tau_1 w_k + \tau_3 z_k(\mathbf{x})\right] + mb_k\log\left[\tau_2 w_k + \tau_4 z_k(\mathbf{x})\right]\right)\right\} \tag{40}$$

which can be formulated to a likelihood function

$$[\hat{\mathbf{w}},\hat{\mathbf{x}}] = \underset{\hat{\mathbf{w}},\hat{\mathbf{x}}\geq 0}{Arg\max}\left\{\mathrm{L}(\hat{\mathbf{w}},\hat{\mathbf{x}})\right\} \tag{39}$$

The background measurement w_k could be solved for directly with the optimization algorithm, but since w_k appears only in the k^{th} term the maximizing value of w_k can be solved for directly. This will reduce the number of variables for which a solution must be found. Assuming that mp_k, mb_k, and $z_k(\mathrm{x})$ are all non-negative the second derivative of $\mathrm{L}(\hat{\mathbf{w}},\hat{\mathbf{x}})$ with respect to w_k is concave for $w_k \geq 0$. So if the first derivative of $\mathrm{L}(\hat{\mathbf{w}},\hat{\mathbf{x}})$ with respect to w_k is set equal to zero and w_k is solved for, the solution will be the global maximizer with respect to w_k. The solutions are given in Equations 41 and 42.

$$w_k = \frac{(-\tau_1\tau_4 - \tau_2\tau_3)z_k(\mathbf{x}) + \tau_1\tau_2(mp_k + mb_k) + f_k(z_k(\mathbf{x}))}{2\tau_1\tau_2} \tag{41}$$

$$f_k(z_k(x)) = \sqrt{\tau_1\tau_2^2(mb_k + mp_k) + 2\tau_1\tau_2(\tau_1 - \tau_3)(mp_k + mb_k)z_k(\mathbf{x}) + (\tau_1 - \tau_3)^2 z_k(\mathbf{x})^2} \tag{42}$$

If the value for w_k in Equation 41 is substituted into $\mathrm{L}(\hat{\mathbf{w}},\hat{\mathbf{x}})$, then $\mathrm{L}(\hat{\mathbf{w}},\hat{\mathbf{x}})$ becomes $\mathrm{L}(\hat{\mathbf{x}})$ and it is only dependent on **x**. Equation 39 states that the maximum likelihood function needs to be determined. If a minimizing algorithm is used the negative of the maximum likelihood function will be used

OPTIMIZATION ALGORITHM

The purpose of an optimization algorithm is to find the minimum, or maximum, of a function as accurately and efficiently as possible. In order to understand how an optimizing algorithm works define, $f(\mathbf{x})$, where f is a function of a vector $\mathbf{x}$. Consider $f(\mathbf{x})$ to be a multi-dimensional concave surface whose minimum is being sought. The gradient of the function, $\frac{\partial f(\mathbf{x})}{\partial \mathbf{x}}$, is also a vector. The negative of the gradient at a particular $\mathbf{x}$ will point to the steepest slope of the function at the location. A new value of $\mathbf{x}$ can be determined along this direction which decreases the value of $f(\mathbf{x})$. Then at the new position, or value of $\mathbf{x}$, a new direction, gradient, and the next value of $\mathbf{x}$ are determined. This optimization method is called steepest descent. This is not the most efficient method. The search can end up going in the same direction repeatedly and many matrix multiplications are needed. A method has been developed to determine a set of search directions so that all the directions are conjugate, or orthogonal. Conjugate directions can be considered to be non-interfering directions, each direction is unique. A set of conjugate directions have the special property that minimization along one direction is not spoiled by the subsequent minimization along another direction in the set[4]. This method is called Conjugate Gradient (CG)[5]

CONSTRAINED CONJUGATE GRADIENT

Constrained Conjugate Gradient (CCG) allows the addition of constraints on the values of the vector $\mathbf{x}$ to the CG optimization method. The user supplies vectors of minimum and maximum values for $\hat{\mathbf{x}}$. For example, in the waste drum case $\mathbf{x} \geq 0$, so the minimum is 0.0 (or a very small number, such as 10^{-10}). The maximum will be set to a very large number, such as 10^{+25}. At each step when the new values for $\hat{\mathbf{x}}$ are calculated each new value is checked against the constraints. If the constraints are exceeded for a x_v, where v is a voxel in $\mathbf{x}$, the value of x_v is change to the constraint value. The effect of adding constraints to CG is to reduce the degrees-of-freedom in the problem and improve the likelihood of finding an effective solution.

The basic steps in the CCG algorithm are shown in Figure 16. x_v^i represents the value for $\mathbf{x}$ for the voxel v for the i^{th} iteration. The first step is to set initial values for $\hat{\mathbf{x}}$. These initial values are checked against the constraints. Any value of $\hat{\mathbf{x}}$ that exceeds a constraint will be set to the constraint. Then the values for $\mathrm{L}(\hat{\mathbf{x}})$,. and $\mathbf{z}(\hat{\mathbf{x}}) = \mathbf{A}\hat{\mathbf{x}}$ are calculated. The next step is to calculate the gradient of the cost function, $\mathrm{L}(\hat{\mathbf{x}})$, with respect to $\hat{\mathbf{x}}$ at the initial value of $\hat{\mathbf{x}}$. The gradient in the waste drum case, where $\mathbf{z}(\hat{\mathbf{x}}) = \mathbf{A}\hat{\mathbf{x}}$ is

$$\mathbf{g} = \nabla_{\mathbf{x}} \mathbf{L}[\mathbf{x}] = \mathbf{A}^{\mathrm{T}} \frac{\partial \mathbf{L}[\mathbf{x}]}{\partial \mathbf{z}} \tag{43}$$

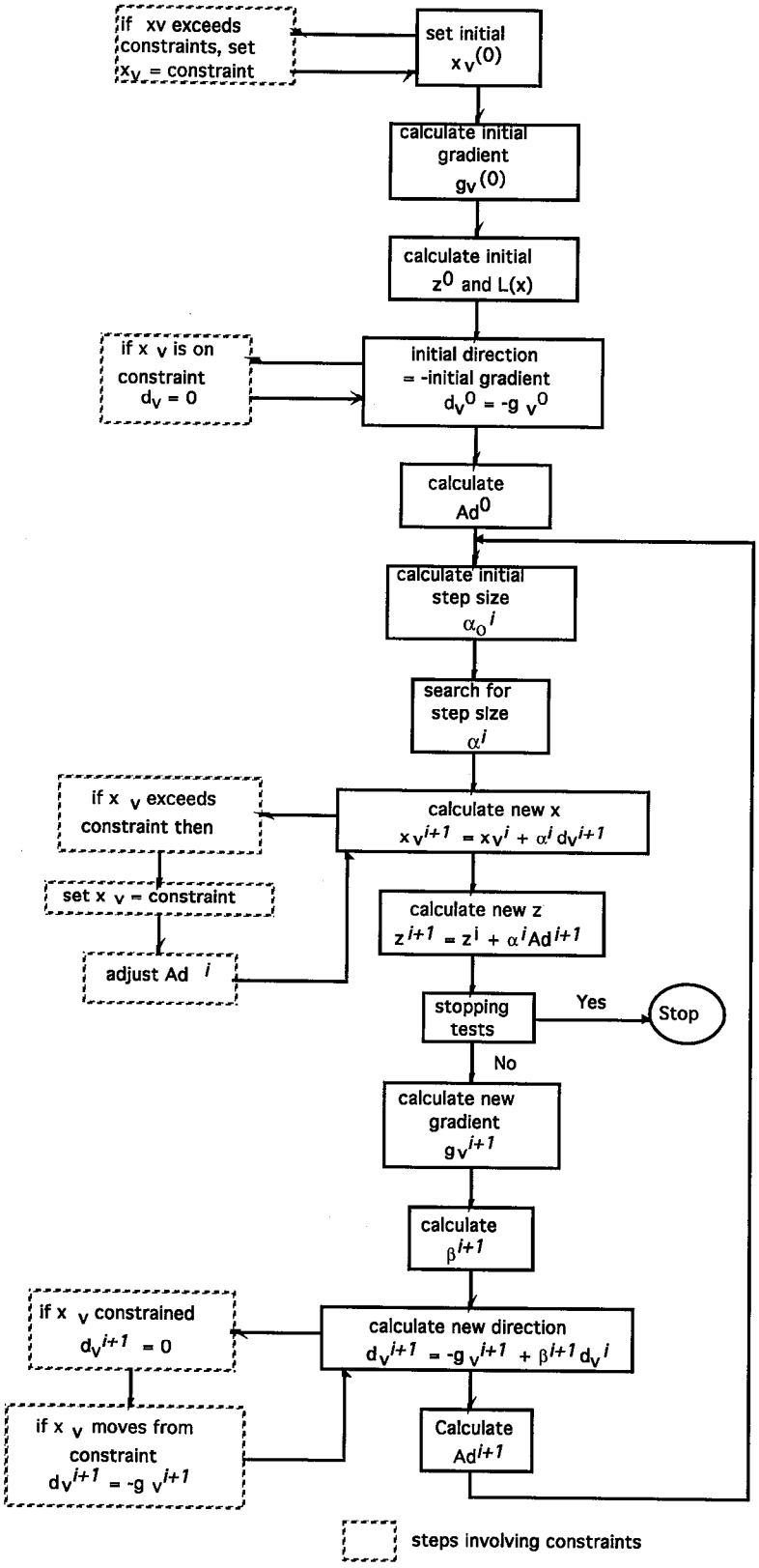

Figure 16: CCG Algorithm

The initial direction, **d,** will be the negative of the gradient

$$\mathbf{d}^0 = -\mathbf{g}^0 \tag{44}$$

If the initial value of x_v was on a constraint $d_v^0 = 0$. Now the matrix multiplication $\mathbf{Ad}^0$ is performed. An important factor to note here is that the matrix operation $\mathbf{Ad}^i$ can be calculated once to form a vector and that vector can be used in multiple occurrences in the algoritm instead of repeating the matrix operations. The next value of x_v^{i+1} is the previous value of $x^{(i)}$ plus a movement in the direction of d^i

$$x_v^{i+1} = x_v^i + \alpha^{i+1} d_v^i \tag{45}$$

where α is defined as the step size. This step size is determined using a line search to find the α that produces the smallest -L(**x**) in the given direction. The initial step size is selected using a 1-D Newton estimate.

$$\alpha_0^i = \frac{\left.\dfrac{\partial \mathrm{L}[\mathbf{x}(\alpha)]}{\partial \alpha}\right|_{\alpha=0}}{\left.\dfrac{\partial^2 \mathrm{L}[\mathbf{x}(\alpha)]}{\partial \alpha^2}\right|_{\alpha=0}} \tag{47}$$

Where $\mathbf{x}(\alpha) = \mathbf{x}^i + \alpha\mathbf{d}^i$ and

$$\frac{\partial \mathrm{L}[\mathbf{x}(\alpha)]}{\partial \alpha} = \frac{\partial \mathrm{L}[\mathbf{x}(\alpha)]}{\partial \mathbf{z}} \mathbf{Ad}^i \tag{48}$$

$$\frac{\partial^2 \mathrm{L}[\mathbf{x}(\alpha)]}{\partial \alpha^2} = \frac{\partial^2 \mathrm{L}[\mathbf{x}(\alpha)]}{\partial \mathbf{z}^2} \left(\mathbf{Ad}^i\right)^{\mathrm{T}} \left(\mathbf{Ad}^i\right) \tag{49}$$

After the line search and α^i is determined the new $\mathbf{x}^{i+1}$ is calculated using Equation 45. After $\mathbf{x}^{i+1}$ is determined the values of $\mathbf{x}^{i+1}$ is checked against the constraints. If any constraints are exceeded the value x_v^{i+1} is set to the constraint, the direction d_v^i is set to 0, and the corresponding value in **is** to be corrected. The correction of $\mathbf{Ad}^i$ only involves recalculating one column in $\mathbf{Ad}^i$. Next the updated value for **z(x)** is calculated. Instead of calculating the matrix operation **z(x) = Ax**, $\mathbf{z}^{i+1}$ can be determined as shown in Equation 50.

$$\begin{aligned} \mathbf{z}^{i+1} &= \mathbf{A}\left(\mathbf{x}^i + \alpha^i \mathbf{d}^i\right) \\ \mathbf{z}^{i+1} &= \mathbf{A}\mathbf{x}^i + \alpha^i \mathbf{A}\mathbf{d}^i \\ \mathbf{z}^{i+1} &= \mathbf{z}^i + \alpha^i \mathbf{A}\mathbf{d}^i \end{aligned} \tag{50}$$

Note that once again the previously determined vector $\mathbf{Ad}^j$ can be used. At this point various stopping criteria are checked. If any of the criteria are satisfied the iterative process is ended.

Now the next conjugate direction $\mathbf{d}^{i+1}$ must be determined. First the gradient, $\mathbf{g}^{i+1}$, at the new location $\mathbf{x}^{i+1}$ is be calculated. Then

$$d_v^{i+1} = -g_v^{i+1} + \beta^{i+1} d_v^{i+1} \tag{51}$$

β^{i+1} is determined by the Gram-Schmidt technique

$$\beta^{i+1} = \frac{\sum g_v^{i+1}\left(g_v^{i+1} - g_v^{i}\right)}{\sum g_v^{i} g_v^{i}} \tag{52}$$

β^{i+1} will create a direction $\mathbf{d}^{i+1}$ that is orthogonal to all previous directions. Once β^{i+1} and d_v^{i+1} are calculated the values of d_v^{i+1} must be checked to see if the direction is moveing x_v away from a constraint. If this is the case the direction is set as

$$d_v^{i+1} = -g_v^{i+1} \tag{53}$$

With the new direction vector, **d**, the process will repeat until the stopping criteria are met and the final value for reconstructed emission image, $\hat{\mathbf{x}}$, is found.

ASSAY CALCULATION

After the reconstructed emission image, **x**, is determined the total assay for the waste drum can be calculated by summing the counts in all the voxels of **x**. The activity and mass values can then be determined from the counts.

$$\text{Total counts (cts)} = \sum_v x(v) \tag{54}$$

$$\text{Activity (miC)} = \frac{total\_counts(cts)}{raytime(secs) \bullet deff \bullet bratio \bullet 3.7\text{x}10^7 (\frac{cts/s}{miC})} \tag{55}$$

$$\text{Mass (gm)} = \frac{activity(miC)}{spact(\frac{miC}{miC/gm})} \tag{56}$$

RESULTS

The reconstruction code currently in use in the LLNL A&PCT system is UCSF-MLEM. UCSF is the model code. It was adapted from a UCSF code specifically designed for medical imaging geometries. LLNL developed a 3-dimensional version and added a Maximum Likelihood Expectation Maximization (MLEM) optimization method. There are several assumptions in the UCSF model code which were valid for the medical imaging case but not for the drum imaging problem. An effort was begun at LLNL to develop a model code that would be more appropriate for the waste drum problem. The resulting model code, described in this paper, is called APCT. This code was originally connected to the MLEM optimization method to create a code called APCT-MLEM.

The optimization method MLEM was based on work also done in the medical community[6]. It was originally designed to work with a one Poisson measurement case. The conversion to a two Poisson measurement case is not entirely effective.

Two biases have been noticed in the assay results when the UCSF-MLEM code is used to reconstruct and provide assay results for passive CT data. One bias is positive and seems to occur for poor statistical data. The other bias is negative and it is of the order of minus 30%, and seems to occur for good statistical data. The research work on the APCT model and CCG optimization codes was performed to reduce both biases.

To better understand the positive bias problem and to determine if the new codes help reduce this bias we have simulated several cases. Simulated sinogram data can be generated from a forward projection of a test image through the APCT model code. When the same model code is used in the forward projection and in the optimization any differences in the results will be due to the effects of the optimization process. Since the APCT-MLEM and APCT-CCG codes use the same model code the effectiveness of the optimization methods, MLEM and CCG, can be compared.

The test cases were generated using a simulated 3-D image with three slices. Each slice was 14 by 14 voxels. A point radioactive emission source of selected counts was placed on the center slice at voxel location (5, 5), i.e., just off the center of the slice. Using the system matrix, **A** generated by the APCT model code, the image was forward projected to create net counts for all the detectors for each slice. A level background of selected counts was then added to these net counts. The simulated signals were randomized by passing them through a Poisson random generator to create the peak measurements.. The background measurements were created by randomizing the same background level.

As discussed earlier the peak signal consists of two components, the background and the net. The net is the contribution from the emission image. The desired result of the optimization process is the emission image that produces the net signal. Although it is statistically incorrect, for Poisson signals, to subtract background counts from peak counts to determine the net counts, for analysis purposes it is useful to determine the average peak counts per detector and the average background counts per detector and take the difference as the average net counts per detector. Measurements from actual data sets were examined to determine the range of average counts per detector to be expected. Then a series of simulations were done to examine the effectiveness of MLEM and CCG under different conditions. Three average background counts per detector levels were used; 1, 5 and 20. The simulated average net counts was achieved by selecting a value for the point emission source in the simulated image that yielded the desired average net counts. For each of the average background levels six average net counts were used; 0.5, 1.0, 2.0, 3.0, 4.0 and 5.0. This allowed examination of the effect of low counts on the optimization codes as well as the effect of the net-to-background ratio.

Figure 17 shows the results of these simulations. At least four points can be made. For net counts greater than one APCT-CCG performs 20% better than APCT-MLEM. APCT-CCG's performance is degraded when the counts are too low. The average net-to-background ratio has almost no effect on the result for either optimization case. For the case of average background of 20 and average net counts of 0.5 and 1.0, APCT-MLEM fails.

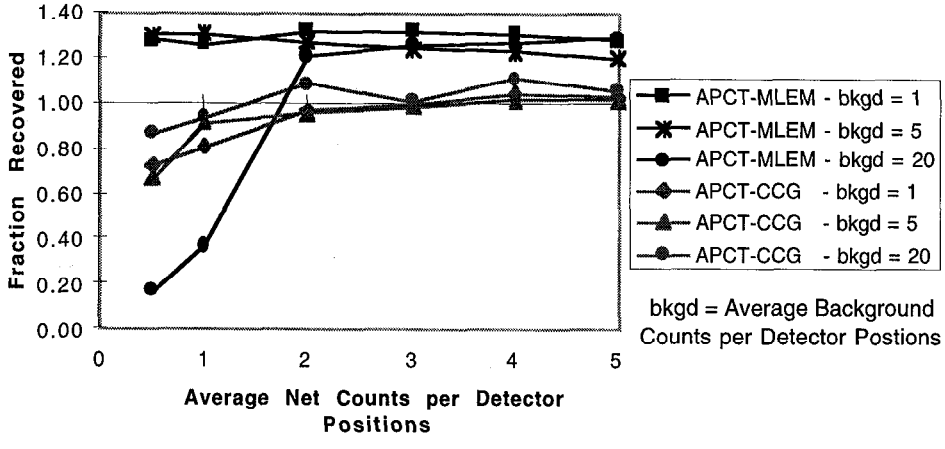

Figure 17: Comparison of Optimization Methods (MLEM and CCG) with Simulated Data

The results of this simulation cannot be quantitatively applied to real data. The average counts per detector will vary with the number of slices in the drum, the position of the emitter in the drum and the amount of attenuation in the drum.

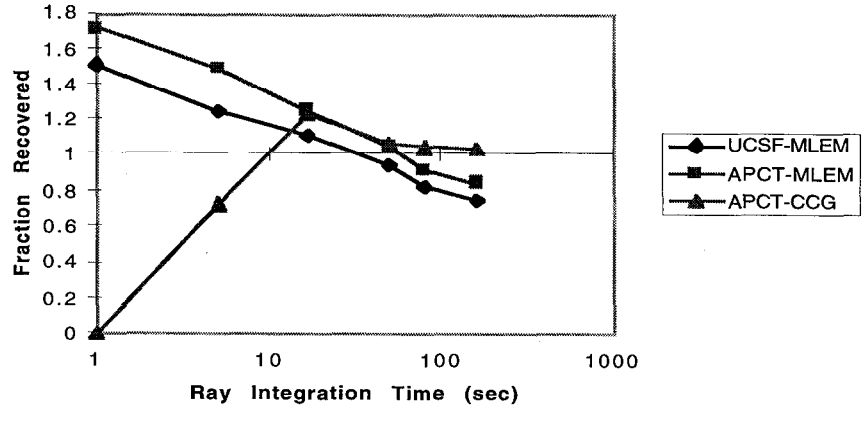

Figure 18: PDP Cycle 2 - 0,93 gram Drum Results vs. Raytime

Figure 18 shows the results of an experiment on real measured data similar to the preceding simulation. In this case a PDP drum with 0.93 grams was scanned for different ray integration times. The average net count to average background count ratio was approximately 1.8 for all ray integration times. As in the simulation, APCT-CCG out performs the other codes when there are enough counts, however it does not perform well when not enough counts are available,.

Finally all the codes were used on several empirical data sets to determine and compare their assay performance. Figure 19 shows a comparison of all three A&PCT codes based on fraction recovered from the calculated and known assay values for various empirical validation data sets. With respect to this figure the empirical data is as follows: c15g20 and o15g20 are abbreviations for a 15-gram ^{239}Pu PDP (Performance Demonstration Program) standard source on the center-axis-of-rotation (c) and off the center axis (o), respectively, with no attenuates and 20-sec. ray-sum integration; pdp_160, 80, and 50

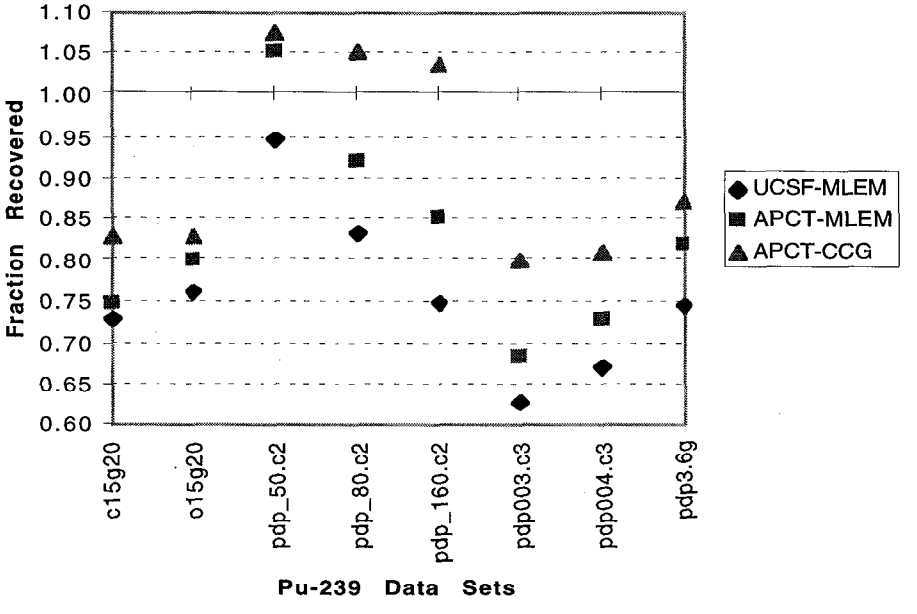

Figure 19: Comparison of Reconstruction Methods

represent the same PDP standards (0.93 grams of ^{239}Pu) within an ethafoam matrix drum with ray-sum integration times of 160, 80, and 50 seconds, respectively. pdp003.c3 and pdp004.c3 are PDP drums from the cycle 3 tests. Their gram levels are 71 grams of ^{239}Pu and 98 grams of ^{239}Pu respectively. pdp3.5g is a 3.6 gram ^{239}Pu drum. From these figures it can be seen that the APCT-MLEM code performs somewhat better than the UCSF-MLEM code. This difference reflects improvements in the model code. The APCT-CCG code performs, on average, better than both MLEM optimization codes. The difference between APCT-MLEM and APCT-CCG reflects the effect of the optimization algorithm.

ACKNOWLEDGMENTS

The algorithm and initial major code development for the system model was done by Eric Keto and Erik Johansson. Erik Johansson was also responsible for the code development of CCG.
This work was performed under the auspices of the U.S. Department of Energy by the Lawrence Livermore National Laboratory under contract W-7405-ENG-48.

REFERENCES

1. T.F. Budinger, G.T. Gullberg, and R.H. Huesman, "Emission Computed Tomography", *Image Reconstrction from Projections Implementation and Applications*, G.T. Herman, Editor, Springer-Verlag, New York, 1979, p.147.

2. Van Trees, H.L., *Detection, Estimation and Modulation Theory, Part I,* John Wiley and Sons, New York, 1968.

3. D.M. Goodman, "Maximum Likelihood Estimation with Poisson Statistics for Waste Drum Inspection", (UCRL-ID-127361), LLNL, Livermore, Ca., May 1997.

4. Press, W.H., Flannery, B.P., Teukolsky, S.A., and Vetterling, W.T., *Numerical Recipes in C*, Cambridge University Press, 1988.

5. J.R.Shewchuk, "An Introduction to the Conjugate Gradient Method without the Agonizing Pain", Carnegie Mellon University, Pittsburg, PA., August 4, 1994.

6. L.A.Shepp and Y.Vardi, "Maximum Likelihood Reconstruction for Emission Tomography", *IEEE Transaction on Medical Imaging*, vol. MI-1,. No. 2, October 1982, pp 113-122.